crystals

MDPI

Article

Crystal Structure, Hirshfeld Surface Analysis, In-Silico and Antimycotic Investigations of Methyl 6-methyl-4-(4-nitrophenyl)-2-oxo-1,2-dihydropyrimidine-5-carboxylate

Alakbar Huseynzada [1,2,3,*], Matteo Mori [4], Fiorella Meneghetti [4], Aygun Israyilova [2,5,6], Elif Guney [7], Koray Sayin [7], Laurent R. Chiarelli [8], Mustafa Demiralp [9], Ulviyya Hasanova [1,2] and Vagif Abbasov [10]

1 "Industrial Chemistry" Research Laboratory, Baku State University, Z. Khalilov 23, Baku AZ1148, Azerbaijan
2 GPOGC SRI, Azerbaijan State Oil and Industry University, Baku AZ1148, Azerbaijan
3 Chemistry Department, Azerbaijan Engineers Union, Bashir Safaroglu 118, Baku AZ1009, Azerbaijan
4 Department of Pharmaceutical Sciences, University of Milan, Via L. Mangiagalli 25, 20133 Milano, Italy
5 Laboratory of Microbiology and Virology, Baku State University, Z. Khalilov 23, Baku AZ1148, Azerbaijan
6 Research Institute of Crop Husbandry, Ministry of Agriculture, Baku AZ1098, Azerbaijan
7 Chemistry Department, Faculty of Science, Sivas Cumhuriyet University, Sivas 58140, Turkey
8 Department of Biology and Biotechnology, University of Pavia, Via A. Ferrata 9, 27100 Pavia, Italy
9 Advanced Technology Research and Application Center, Sivas Cumhuriyet University, Sivas 58140, Turkey
10 Institute of Petrochemical Processes, K. Avenue 30, Baku AZ1005, Azerbaijan
* Correspondence: alakbar.huseynzada1117@gmail.com

Abstract: Herein, we report the preparation of methyl 6-methyl-4-(4-nitrophenyl)-2-oxo-1,2-dihydropyrimidine-5-carboxylate **2**, obtained by the regioselective oxidative dehydrogenation of the dihydropyrimidine derivative **1** in the presence of cerium ammonium nitrate. The structure of compound **2** was investigated by single-crystal X-ray diffraction (SC-XRD), which allowed the determination of its tautomeric form. Moreover, the presence of non-covalent interactions and their impact on the crystal structure were analyzed. To better characterize the intermolecular contacts, the Hirshfeld surface and enrichment ratio analyses were performed. Furthermore, the antimycotic activity of compounds **1** and **2** was investigated against *Candida albicans*, *Aspergillus flavus*, and *Aspergillus niger*, and their efficacy was compared to that of fluconazole. Computational investigations on the putative target of the compounds provided insights to explain the better activity of **2** with respect to its synthetic precursor.

Keywords: 1,2-dihydropyrimidines; regioselective oxidation; intramolecular hydrogen bonds; Hirshfeld surface analysis; molecular docking; antimycotic activity

Citation: Huseynzada, A.; Mori, M.; Meneghetti, F.; Israyilova, A.; Guney, E.; Sayin, K.; Chiarelli, L.R.; Demiralp, M.; Hasanova, U.; Abbasov, V. Crystal Structure, Hirshfeld Surface Analysis, In-Silico and Antimycotic Investigations of Methyl 6-methyl-4-(4-nitrophenyl)-2-oxo-1,2-dihydropyrimidine-5-carboxylate. *Crystals* **2023**, *13*, 52. https://doi.org/10.3390/cryst13010052

Academic Editor: Duane Choquesillo-Lazarte

Received: 2 October 2022
Revised: 4 December 2022
Accepted: 19 December 2022
Published: 27 December 2022

1. Introduction

Since its discovery by the Italian chemist Pietro Biginelli at the end of the XIX century, the Biginelli reaction has played a fundamental role in the synthesis of numerous biologically active heterocycles [1]. This reaction is an example of a one-pot three-component condensation involving an aldehyde, a methylene active compound and a urea derivative, with the catalysis of a Brønsted-Lowry or Lewis acid [2,3]. The products of this reaction are dihydropyrimidines, six-membered nitrogen-containing heterocycles that have found several applications in the pharmaceutical and chemical industry [4]. Moreover, their remarkable biological activities have made this class of compounds an essential source of scaffolds for the medicinal chemistry field [5]. In detail, natural and synthetic dihydropyrimidine derivatives have proved to possess antiviral [6,7], antiproliferative [8,9], antitumor [10–15], antibacterial [16–22], anti-inflammatory [23–26], antitubercular [27,28], antifungal [29], anti-leishmanial [30], anti-hypertensive [31–33], antiepileptic [34], antidiabetic [35–38], anti-HIV [39], antimalarial [40], larvicidal [41], and many other [42–44] activities. They have also been described as antagonists of the calcium [31,45] and potassium

channels [46–48], and of the α_{1a}-adrenergic receptor [49]. Most notably, dihydropyrimidines also constitute the core structure of several approved drugs, including batzelladine A and B (against HIV) [39], monastrol, enastron, mon-97, fluorastrol (against cancer) [10–15], and terazosin (against benign prostatic hyperplasia and high blood pressure) [43]. Overall, these remarkable results have fueled the research on dihydropyrimidine chemistry, leading to the discovery of new synthetic methods and inspiring structural modifications. Among them, the oxidation of the heterocyclic nucleus occupies a special position because it was shown to enhance the biological activity of the dihydropyrimidine core and improve its solubility. In addition, oxidized products present some peculiar structural features; for instance, they exist as tautomers in solution (Figure 1) [50].

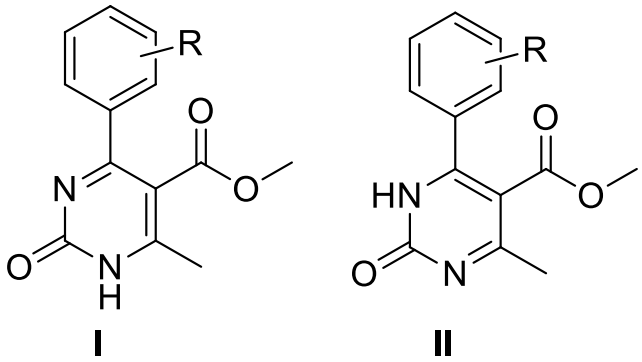

Figure 1. Tautomeric forms of oxidized dihydropyrimidines.

Interestingly, due to the presence of non-covalent interactions in the molecular structure, only one tautomer is detectable in the solution. This feature, typical of the oxidized dihydropyrimidine core, has an impact on the chemical behavior of the compounds, as well as on their activity. Hence, the study of these derivatives is crucial for the comprehension of the structure-activity relationships of this class of compounds [51].

In light of these considerations, we performed an investigation of methyl 6-methyl-4-(4-nitrophenyl)-2-oxo-1,2-dihydropyrimidine-5-carboxylate **2**, obtained by the regioselective oxidative dehydrogenation of the dihydropyrimidine derivative **1**, in the presence of cerium ammonium nitrate (CAN). The title compound **2** was investigated by NMR, and SC-XRD to determine its tautomeric form. Furthermore, the presence of non-covalent interactions and their impact on the crystal packing was examined with the support of Hirshfeld surface and contact enrichment analyses. The structural characterization was supplemented by computational studies, performed by using DFT methods. Additionally, the biological activity of compounds **1** and **2** was assayed against *Candida albicans*, *Aspergillus flavus*, and *Aspergillus niger* and compared to that of fluconazole. Finally, the antimycotic effect of these compounds was studied by preliminary molecular docking calculations against a putative target.

2. Materials and Methods

2.1. General Information

All the solvents and reagents, purchased from commercial suppliers, were of analytical grade and used without further purification. The control of the reaction progress and the determination of the purity of the synthesized compounds were performed by thin-layer chromatography (TLC) on Merck silica gel plates (60 F254 aluminum sheets; Merck, Darmstadt, Germany), visualized under UV light. Melting points were recorded in open capillary tubes on a Büchi B-540 apparatus (Büchi Labortechnik, Flawil, Switzerland) and were uncorrected. Elemental analysis was performed on a Carlo Erba 1108 analyzer (Carlo Erba, Cornaredo, Italy).

2.2. Synthesis

The synthesis of compounds **1** and **2** was performed following a literature procedure [50].

Methyl 6-methyl-4-(4-nitrophenyl)-2-oxo-1,2,3,4-tetrahydropyrimidine-5-carboxylate (1). 4-Nitrobenzaldehyde (76 mg, 0.5 mmol), urea (45 mg, 0.75 mmol), and $Cu(OTf)_2$ (30 mg, 0.08 mmol) were added to a microwave vial equipped with a magnetic stirrer and dissolved in 1 mL of EtOH (Figure 2). Subsequently, methyl acetoacetate (50 µL, 0.46 mmol) was added, and the mixture was irradiated at 100 °C in a microwave reactor for 2.5 h at a maximum power of 200 W (CEM Discover^{TM} System; CEM, Buckingham, UK). After completion, the reaction was poured on ice; the resulting precipitate was filtered, washed with distilled water, and dried to afford the title compounds **1** as a white solid. In the absence of a precipitate, the reaction was allowed to stand on ice overnight. Yield: 72%. M.p.: 235–237 °C. ^{1}H NMR (DMSO-d_6, δ, ppm): 2.27 (s, 3H, CH_3), 3.54 (s, 3H, OCH_3), 5.28–5.29 (d, *J* = 3 Hz, 1H, CH), 7.5–7.53 (d, *J* = 9 Hz, 2H, H_{Ar}), 7.88 (s, 1H, NH), 8.2–8.22 (d, *J* = 6 Hz, 2H, H_{Ar}), 9.35 (s, 1H, NH). ^{13}C NMR (DMSO-d_6, δ, ppm): 18.25 (CH_3), 51.23 (CH), 53.91 (OCH_3), 98.39 (C), 124.19 ($2C_{Ar}H$), 127.93 ($2C_{Ar}H$), 147.11 (C), 149.94 (C_{Ar}), 152.13 (C_{Ar}), 152.16 (COO), 165.92 (CO). Elemental analysis calcd. for $C_{13}H_{13}N_3O_5$, %: C, 53.61; H, 4.50; N, 14.43. Found, %: C, 53.66; H, 4.54; N, 14.40. Analytical data agree with the reported literature values [50].

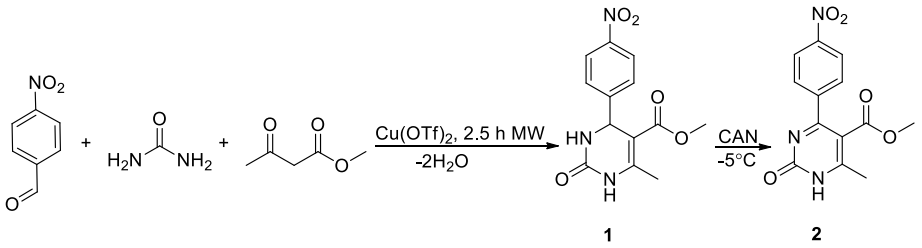

Figure 2. Synthesis of compounds **1** and **2**.

Methyl 6-methyl-4-(4-nitrophenyl)-2-oxo-1,2-dihydropyrimidine-5-carboxylate (2). Dihydropyrimidine **1** (87 mg, 0.30 mmol) was dissolved in a solvent mixture consisting of 4 mL of DMSO and 4 mL of acetone. To this solution, $NaHCO_3$ (168 mg, 2 mmol) was added, and the reaction mixture was cooled to −5 °C. Then, CAN (658 mg, 1.2 mmol) was dissolved in 2 mL of water and added to the solution under argon (Ar) atmosphere, leading to a colour change from orange to pale-yellow. The reaction was stirred for 1 h at −5 °C and for 20 h at room temperature (Figure 2). Then, the mixture was decanted with $CHCl_3$. Subsequently, the organic layer was washed with brine and dried over anhydrous Na_2SO_4. The removal of the solvent gave a precipitate, which was further purified with a Biotage Isolera One (Biotage, Uppsala, Sweden) flash chromatography system (EtOAc-MeOH 9:1), allowing the obtainment of the pure oxidized dihydropyrimidine **2** as a white solid. Yield: 28%. M.p.: 210–211 °C. ^{1}H NMR (DMSO-d_6, δ, ppm): 2.46 (s, 3H, CH_3), 3.49 (s, 3H, OCH_3), 7.68–7.71 (d, *J* = 9 Hz, 2H, H_{Ar}), 8.30–8.33 (d, *J* = 9 Hz, 2H, H_{Ar}), 12.62 (s, 1H, NH). ^{13}C NMR (DMSO-d_6, δ, ppm): 28.99 (CH_3), 51.98 (OCH_3), 123.42 ($2C_{Ar}H$), 128.87 ($2C_{Ar}H$), 144.82 (C), 148.12 (C), 154.69 (C), 154.90 (C_{Ar}), 161.83 (C_{Ar}), 162.12 (COO), 165.60 (CO). Elemental analysis calcd. for $C_{13}H_{11}N_3O_5$, %: C, 53.98; H, 3.83; N, 14.53. Found, %: C, 53.91; H, 3.89; N, 14.57. Analytical data agree with the reported literature values [50].

2.3. NMR Experiments

NMR experiments were performed on a Bruker AVANCE 300 FT-NMR spectrometer (Bruker, Karlsruhe, Germany), operating at 300 MHz for ^{1}H and 75 MHz for ^{13}C, and equipped with a BVT 3200 variable temperature unit. Acquisitions were carried out in 5 mm sample tubes using Bruker Standard software (TopSpin 3.1). Chemical shifts are given in ppm (δ) and are referenced to internal tetramethylsilane (TMS). Coupling constants *J* are given in Hz. The experimental parameters for ^{1}H are as follows: digital resolution =

0.23 Hz, SWH = 7530 Hz, TD = 32 K, SI = 16 K, 90° pulse-length = 10 ms, PL1 = 3 dB, ns = 1, ds = 1, d1 = 1 s; for ^{13}C: digital resolution = 0.27 Hz, SWH = 17,985 Hz, TD = 64 K, SI = 32 K, 90° pulse-length = 9 ms, PL1 = 1.5 dB, ns = 1500, ds = 2, d1 = 3 s. NMR-grade DMSO-d_6 (99.7%, containing 0.3% H_2O) was used to solubilize the synthesized compounds **1** and **2**.

2.4. X-ray Analysis

X-ray analyses were performed on a Bruker SMART APEX II Single Crystal X-ray Diffractometer (Bruker, Karlsruhe, Germany), equipped with graphite-monochromated Mo-Kα radiation (λ = 0.71073 Å) at 296(2) K. The crystal structure was solved by direct methods and refined on F^2 by full-matrix least-squares using Bruker's SHELXTL-97 [52]. Details are summarized in Table 1. Crystallographic data were deposited to the Cambridge Crystallographic Data Center under accession number CCDC 2040960. The refined structure was inspected using ORTEP-3 (v. 2020.1) [53] and analyzed by Mercury 4.0 (v. 2021.3.0) [54] and PARST [55], within the WinGX suite (v. 2021.3) [53]. Graphical representations were rendered with Mercury.

Table 1. Crystal data and structural parameters of compound **2**.

Crystal Data	
Chemical formula	$C_{13}H_{11}N_3O_5$
M_r	289.25
Crystal system, space group	Triclinic, P-1
a, b, c (Å)	7.2632(7), 8.4463(9), 11.1188(11)
α, β, γ (°)	69.202(2), 88.714(2), 88.195(2)
V (Å^3)	637.30(11)
Z	2
F(000)	300
Density (g/cm^3)	1.507
Temperature (K)	298
Radiation type	Mo-Kα (λ = 0.71073 Å)
μ (mm^{-1})	0.119
Crystal size (mm)	0.504 × 0.132 × 0.086
Data collection	
Diffractometer	Bruker-Axs Smart-Apex CCD
T_{min}, T_{max}	0.369, 0.746
No. of measured, independent andobserved [$I > 2\sigma(I)$] reflections	5949, 2228, 1727
R_{int}	0.0453
Structure refinement	
R, wR^2, S	0.0434 [$I > 2\sigma(I)$] and 0.0562 [all], 0.1160 [$I > 2\sigma(I)$] and 0.1227 [all], 1.058 [all]
No. of parameters	192
No. of restraints	0
$\Delta\rho_{max}$, $\Delta\rho_{min}$ (e Å^{-3})	0.181, −0.221

2.5. Hirshfeld Surface Analysis

Hirshfeld surfaces and two-dimensional fingerprint plots were generated using CrystalExplorer21 (v. 21.5) [56]. Contact enrichments were calculated according to Jelsch et al. [57].

2.6. Biological Assay

The antifungal activity of the synthesized dihydropyrimidines **1** and **2** was evaluated against reference strains of *Candida albicans* ATCC 22019, *Aspergillus flavus* ATCC 204304, and a clinical isolate of *Aspergillus niger*, by the microdilution method performed according to the CLSI guidelines [58,59]. Potato Dextrose (PDA) and Sabouraud Dextrose Agar (SDA)

plates were used for the cultivation of molds and yeast cultures, respectively. Agar cultures were used for the preparation of stock fungal suspensions. The mold conidial and yeast cell suspensions were prepared in RPMI 1640 medium (Sigma Aldrich, St. Louis, MO, USA), supplemented with 2% glucose; the density of the cells was adjusted to 1–5 × 10^5 cells/mL, as previously described [58,60]. The 96-well round-bottom microplates were used for determining the MIC of the test compounds. The concentration of the compounds (stock solution prepared in DMSO) ranged between 256 and 2 µg/mL. The inoculated plates were incubated for 48 h at 35 °C, except for *C. albicans*, which was incubated at the same temperature for 24 h. The MIC was determined by adding 0.01% resazurin dye (Sigma Aldrich), prepared in sterile distilled water, followed by re-incubation of the plates for 4–6 h at 35 °C [59]. The lack of color change from blue to pink indicated a growth inhibition induced by the test compounds. Fluconazole was used as the positive control, whereas DMSO was employed as a negative control.

2.7. In Silico Studies

The synthesized compounds were fully optimized at the B3LYP-D3/6-311++G(d,p) level in water. The conductor-like polarizable continuum model (C-PCM) was adopted to consider solute-solvent interactions. IR and NMR spectra of the studied compounds were calculated at the same level of theory. Electronic properties were investigated by calculating the contour plot of frontier molecular orbital and molecular electrostatic potential (MEP) maps. Moreover, to investigate the antifungal activity of the studied compounds against *Aspergillus niger*, molecular docking analyses were performed on the putative target protein chitin deacetylase AngCDA (PDB code: 7BLY). This protein was selected because it plays a key role in the removal of the acetyl group from chitinous substrates, generating various chitosans. Chitosan, a polymer of 1,4-linked glucosamine units, performs several crucial functions in the fungal cell wall, enhancing virulence and facilitating immunological evasion [60,61]. No imaginary frequency was observed in the whole calculation. Computational studies were performed using Gaussian software, while molecular docking calculations were performed using Maestro 12.8. In molecular docking calculations, the OPLS4 method and modules such as LigPrep, ProteinPrep, ReceptorGridGeneration, and LigandDocking were used.

3. Results

3.1. Chemical Synthesis

The key dihydropyrimidine intermediate **1** was obtained by the Biginelli reaction in the presence of copper triflate, a safe and cheap triflate salt (Figure 1). The structural characterization of the synthesized dihydropyrimidine was performed by ^{1}H, ^{13}C NMR spectroscopy and elemental analysis (Figures S1 and S2 see Supplementary materials); experimental data were compared to literature data, which confirmed the obtainment of the desired compound [50]. The signals of the methyl and methoxy groups were observed at 2.27 and 3.54 ppm in the ^{1}H NMR spectrum, whereas in the ^{13}C NMR spectrum the same signals were detected at 18.25 and 53.91 ppm. The CH of the dihydropyrimidine core was observed at 5.28 ppm in the ^{1}H NMR spectrum and at 51.23 ppm in the ^{13}C NMR spectrum. The amine groups had chemical shifts of 7.88 and 9.35 ppm in the ^{1}H NMR spectrum.

The next synthetic step was a regioselective oxidative dehydrogenation in the presence of CAN, which led to the obtainment of the oxidized dihydropyrimidine **2** [50]. The signals of the methyl and methoxy groups shifted to 2.46 and 3.49 ppm in the ^{1}H NMR spectrum (Figure S3), whereas they were detected at 28.99 and 51.98 ppm in the ^{13}C NMR spectrum (Figure S4). The CH of the dihydropyrimidine core disappeared due to the oxidation of the heterocyclic ring. The single amine group was at 12.62 ppm in the ^{1}H NMR spectrum.

According to literature data [50], the oxidized products of dihydropyrimidines can exist in the form of tautomers (Figure 1, R = 4-NO_2).

A detailed NMR investigation of compound **2** revealed the absence of signal splitting, suggesting that **2** exists as a single tautomer in solution. Hence, to unambiguously deter-

mine the most stable tautomeric form, single crystals of **2** were grown and analyzed by SC-XRD. This study demonstrated that **2** exists in the tautomeric form **I**; more details are provided in the next section.

3.2. Structure Description

Single crystals of the title compound were obtained by the slow evaporation of a MeOH-EtOAc-cyclohexane (8:1:1) solution after 4 weeks. Crystallographic data and refinement details are given in Table 1.

Compound **2** crystallized in the triclinic space group P-1; its structure is shown in Figure 3 as an ORTEP diagram [53], indicating the arbitrary atom-numbering scheme used in the following discussion.

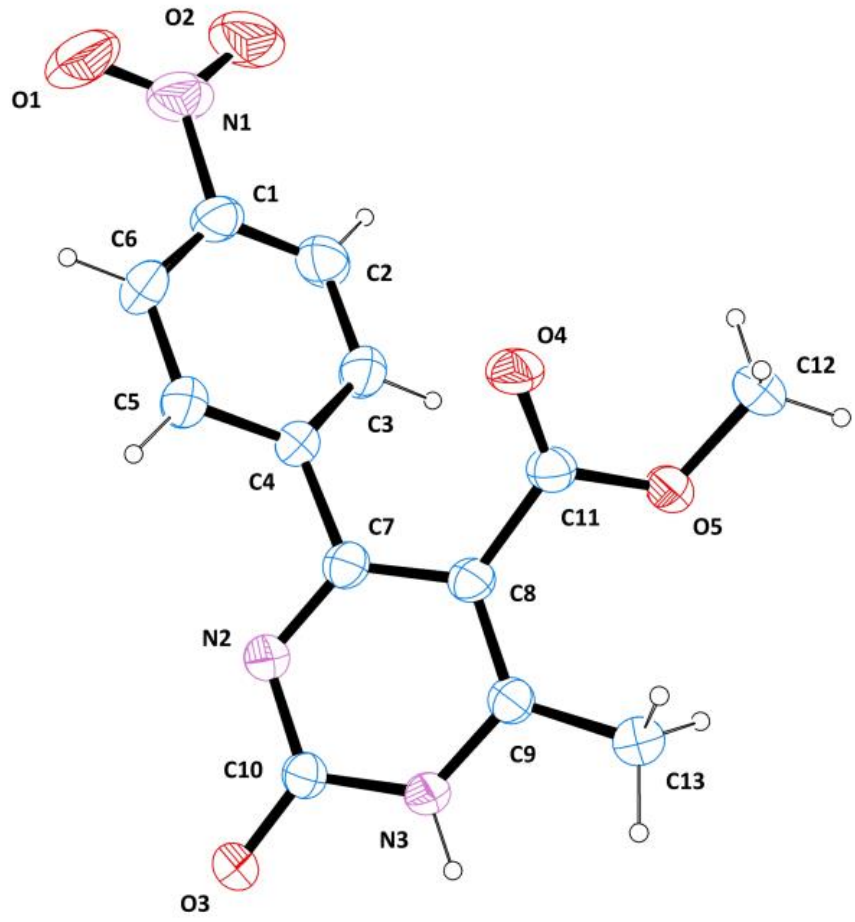

Figure 3. ORTEP diagram of **2**, with the arbitrary atom-numbering scheme. Thermal ellipsoids are drawn at the 40% probability level.

The molecular structure of **2** is characterized by a dihydropyrimidine nucleus bound to a *p*-nitrophenyl moiety. The angle between the best mean plane calculated for the heterocyclic ring and the aromatic portion is 47.9(1)°, while the dihedral angle C9-C8-C11-O5 is 44.3(3)°. The dihydropyrimidine ring is nearly planar, with a maximum deviation of 0.017(1) Å. The crystal packing is consolidated by strong parallel π-π stacking interactions between the phenyl moieties: the distance between the centroids is 4.03(6) Å, while the angle between the centroid-centroid vector and the plane normal is 17.7(4)°. Dimeric H-bonds involve N3-H3$\cdots$O3^{I} (^{I} at -x, 2-y, 1-z); the donor-acceptor (D$\cdots$A) distance is 2.76(1) Å, the hydrogen and the acceptor (D-H$\cdots$A) are at 1.90(2) Å, and the angle is 176.2(5)°. Loose CH$\cdots$O contacts contribute to the stabilization of the crystal structure; these non-traditional H-bonds are established between C3-H3A$\cdots$O3^{I}, D$\cdots$A = 3.23(8) Å, D-H$\cdots$A = 2.35(1) Å, angle = 159.3(9)°. Figure 4 provides a graphical depiction of the main

intermolecular contacts and a representation of the crystal packing. These intermolecular contacts, and especially the dimeric hydrogen bond (N3-H3$\cdots$O3^{I}), demonstrated the existence of compound **2** in the tautomeric form **I** (Figure 1, R = 4-NO_2).

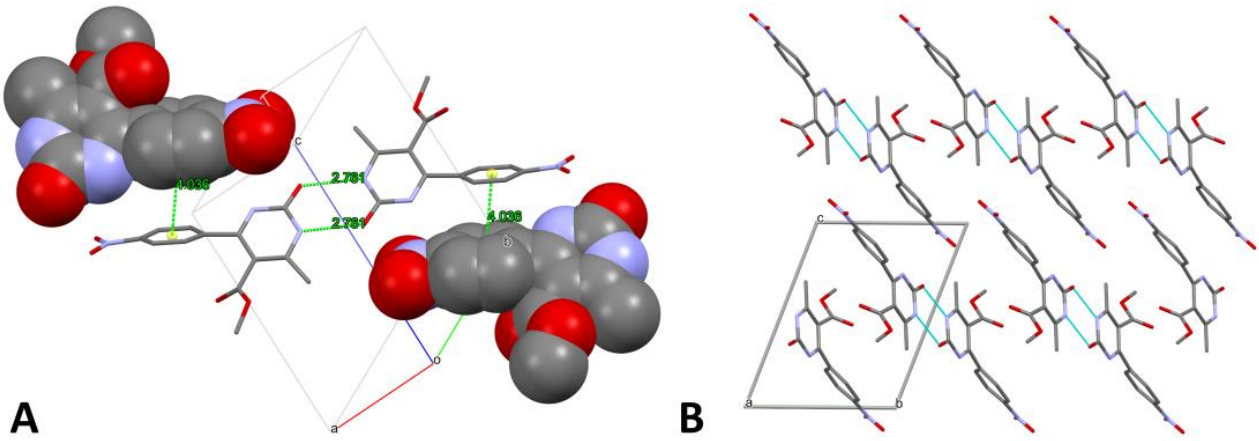

Figure 4. (**A**) Spacefill-stick model of **2** in an arbitrary orientation, evidencing the main H-bonds and the π-π stacking interactions. (**B**) Stick model showing the crystal packing along the *a* axis. Hydrogen atoms are omitted for the sake of clarity.

Of note, the structure of compound **1** was recently solved by Bairagi and collaborators [62] in the framework of a study of dihydropyrimidine co-crystals. The reduced compound **1** crystallized in the same space group as **2** (P-1) and was refined to a similar R factor. The main discrepancies between the two structures are related to the different conformation of the molecules, which is due to the presence of an additional double bond in **2**. As a result, while the oxidized form features a nearly planar heterocycle, the dihydropyrimidine nucleus of **1** takes the shape of a distorted boat. Moreover, the presence of an asymmetric carbon in **1** significantly alters the relative orientation of the heterocyclic and aromatic rings, which assume the typical tetrahedral disposition of the substituents of an sp^3-hybridized carbon. Conversely, the two rings are linked by sp^2 carbons in **2**. The torsion angle N2-C7-C4-C3 is $-133.1(1)^\circ$ in **2**, while the corresponding angle in **1** is $-101.4(1)^\circ$. Interestingly, the orientation of the methyl ester group also changes: in detail, the torsion angle C9-C8-C11-O5 is $44.3(1)^\circ$ in and $-175.9(3)^\circ$ in **1**. The different conformation of the two molecules also affects their arrangement in the crystal: the higher planarity of **2** allows for a tighter packing and results in a slightly lower cell volume (637.30(11) $Å^3$ vs. 659.14(16) $Å^3$). The asymmetric unit of **1** and **2** and an overlay of the two molecules are depicted in Figure 5.

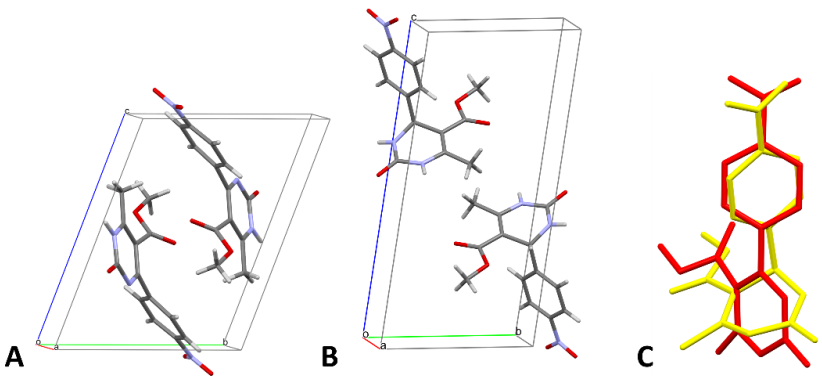

Figure 5. (**A**.) Asymmetric unit of **2**. (**B**.) Asymmetric unit of **1**, according to the crystal structure solved by Bairagi and co-workers [62]. (**C**.) Overlay of **1** (yellow) and **2** (red). Hydrogens are omitted for the sake of clarity.

3.3. Hirshfeld Surface Analysis

The Hirshfeld surface of the title dihydropyrimidine **2** was mapped over the normalized contact distance (d_{norm}), according to the following equation:

$$d_{norm} = \frac{d_i - r_i^{vdW}}{r_i^{vdW}} + \frac{d_e - r_e^{vdW}}{r_e^{vdW}}$$

where d_i is the distance between the HS and the nearest nucleus inside the surface, d_e is the distance between the HS and the nearest nucleus outside the surface, and r^{vdW} represents the van der Waals radius of the atom [63–65]. Details of the HS are provided in Table 2.

Table 2. Characteristics of the HS generated for **2**.

2	V (Å^3)	A (Å^2)	*G*	Ω
HS	312.65	295.94	0.753	0.158

The d_{norm} property was visualized with a red-blue-white color scheme, based on the length of the intermolecular contact with respect to the sum of the van der Waals radii (Figure 6A). The analysis of the surface revealed the presence of two large red spots, corresponding to the short-range H-bond established between N3-H3 and O3. A slightly weaker signal indicated the presence of the non-traditional H-bond between O3 and an aromatic CH of the phenyl ring. The remaining feeble spots represent random short contacts, without chemical significance. The surface mapped over the shape index (SI) showed the typical features of parallel π-π stacking interactions, namely an alternating pattern of red-blue regions on the phenyl ring (Figure 6B). This property also revealed the presence of two hollow areas, one at the center of the aromatic substituent and the other between the dihydropyrimidine nucleus and the ester side chain. The most significant bumps were determined by the ester moiety and the methyl groups; otherwise, the structure appeared to be relatively unperturbed. This was confirmed by the curvedness plot, which showed two large flat areas on one side, and a more irregular surface on the other (Figure 6C).

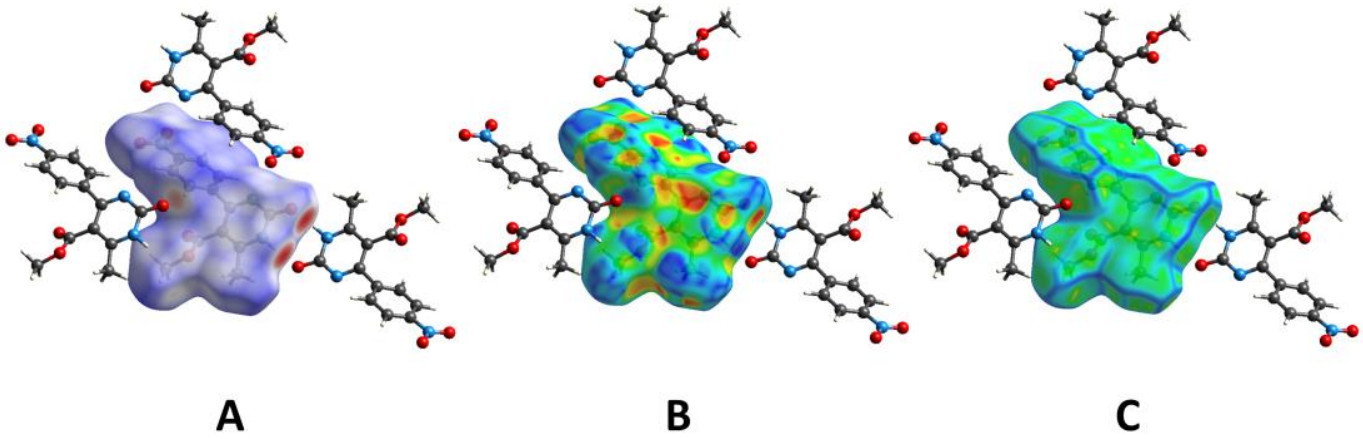

Figure 6. (**A**) HS mapped over d_{norm} with a fixed color scale in the range −0.6640 au (red)–1.1565 au (blue), based on the length of the intermolecular contacts with respect to the sum of the van der Waals radii (red: shorter; blue: longer; white: same). (**B**) HS mapped over the shape-index (color scale: −0.9976 au–0.9959 au). Blue areas represent bumps and red regions indicate hollows. (**C**) HS mapped over the curvedness (color scale: −3.6750 au–0.2678 au). Green represents flat regions and blue indicates edges.

The two-dimensional (2D) fingerprint of the HS (Figure S5), providing a visual summary of the contribution of each contact type and the relative area of the surface corresponding to it, revealed the prominence of O···H/H···O interactions (35.9%), mainly representing

the H-bonds ensuring the stability of the packing. The presence of short-range contacts, due to the N3-H3$\cdots$O3^{I} interactions, was attested by the elongated spikes protruding towards the lower left part of the plot. The characteristic arrow-shaped region in the upper-center area of the fingerprint confirmed the presence of π-π stacking interactions, despite these contacts only accounted for 2.9% of the surface. The remaining contacts occupied more significant portions of the HS, albeit without representing significant chemical interactions. The only exception was constituted by C$\cdots$H/H$\cdots$C contacts in which weak C-H$\cdots\pi$ interactions marginally contributed to the computation of the surface area. These conclusions were supported by the analysis of the contact enrichments (Table 3) [57], which showed that only C$\cdots$C, O$\cdots$H/H$\cdots$O, and C$\cdots$H/H$\cdots$C contacts are enriched ($E_{XY} \geq 1$).

Table 3. Analysis of the intermolecular contacts on the HS of **2**, according to Jelsch et al. [57]. The first part of the table gives the surface contribution S_X of each chemical type *X* to the Hirshfeld surface. The second part shows the proportions of the actual contacts (C_{XY}), and the third part indicates the enrichment ratios (E_{XY}) of the various contact types. Reciprocal contacts X$\cdots$Y and Y$\cdots$X are merged. E_{XY} were not computed when the random contacts (R_{XY}) were lower than 0.9%. E_{XY} ratios larger than unity indicate enriched contacts (in bold), while those lower than unity are impoverished. The percentages of actual contacts were calculated using CrystalExplorer21.5.

.	**Atoms**	**H**	**C**	**N**	**O**
.	*Surface (%)*	55.6	12.0	6.4	26.2
.	*Contacts (%)*				
.	H	27.7			
.	C	13.2	2.9		
.	N	6.6	1.4	1.2	
.	O	35.9	3.5	2.3	5.3
.	*Enrichments*				
.	H	0.9			
.	C	**1.0**	**2.1**		
.	N	0.9	0.9	–	
.	O	**1.2**	0.6	0.7	0.8

3.4. Biological Assays

The antifungal activity of compounds **1** and **2** (minimum inhibitory concentration, MIC, µg/µL) was studied by the microdilution method, according to the CLSI guidelines [58,59,66]. Three fungal strains were employed, namely *Aspergillus niger*, *Aspergillus flavus*, and *Candida albicans*, and fluconazole was used the positive control. As shown in Table 4, both compounds **1** and **2** were active against all the fungal cultures, showing

an efficacy comparable to that of fluconazole. In detail, the activity of compound **1** was equal to that of fluconazole against *A. niger* and *A. flavus*, while it was lower when tested against *C. albicans*. Conversely, *A. niger* and *A. flavus* were found to be more susceptible to compound **2** (MIC = 16 µg/mL) compared to fluconazole, whereas the activity of the dihydropyrimidine **2** against *C. albicans* was analogous to that of the drug (MIC = 32 µg/mL). DMSO was used as a negative control, and no inhibition was detected against the fungal strains. Notably, the antibacterial effect of these compounds has already been screened against different bacterial strains in a previous work by our research group [50], resulting in significantly lower activities compared to those obtained on fungal cultures.

Table 4. MIC (µg/µL) of the studied compounds.

Fungi	MIC		
	1	**2**	**Fluconazole**
Candida albicans	64	32	32
Aspergillus niger	32	16	32
Aspergillus flavus	32	16	32

Our results revealed an improved activity against test cultures of compound **2** compared to **1**. The enhanced antifungal potency of **2** may be related to its chemical structure, particularly to its "more aromatic" ring, which could be responsible for the biological activity. Indeed, the antimicrobial effect of aromatic compounds has been previously observed against different microbial strains [67–70].

3.5. In Silico Analyses

3.5.1. Structure Optimization

The investigated dihydropyrimidine derivatives were optimized at the B3LYP-D3/6-311++G(d,p) level, resulting in the structures shown in Figure 7. Bond lengths (Å), bond angles (degrees), dihedral angles (degrees), and geometric parameters are given in Table 5. The total energy for compounds **1**, **2(I)**, and **2(II)** were calculated to be −754.482651, −746.783920, and −746.782920, respectively. Therefore, **2(I)** proved to be more energetically favored.

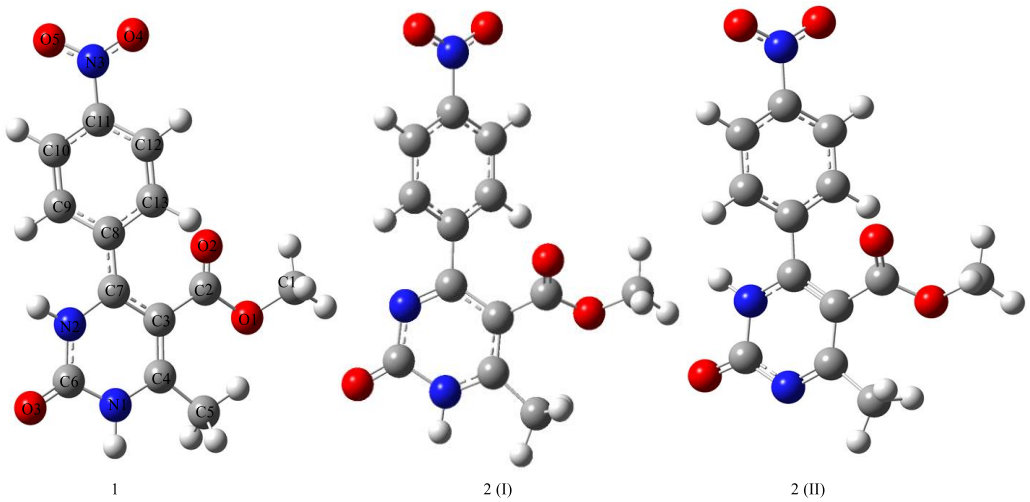

Figure 7. Optimized structure of the investigated compounds.

Table 5. Geometric parameters of the compounds calculated at the B3LYP/6-31+G(d,p) level.

Assignments	1	2 (I)	2 (II)
Bond Lengths(Å)			
C1-O1	1.443	1.445	1.444
C2-O2	1.217	1.215	1.217
C2-C3	1.496	1.485	1.488
C3-C4	1.380	1.386	1.450
C4-C5	1.498	1.503	1.506
C4-N1	1.389	1.353	1.313
C3-C7	1.429	1.446	1.383
C7-C8	1.441	1.491	1.485
C8-C9	1.421	1.402	1.402
C11-N3	1.453	1.475	1.477
N3-O4	1.238	1.232	1.231
Bond Angle (deg)			
C1-O1-C2	115.9	115.4	115.6
O1-C2-O2	123.6	122.9	123.0
O2-C2-C3	125.0	124.1	124.4
C2-C3-C4	118.4	122.1	123.9
C3-C4-C5	127.3	126.0	121.2
C4-N1-C6	125.2	125.2	121.0
N1-C6-O3	122.8	118.8	125.4
N1-C6-N2	113.6	115.6	115.8
N2-C7-C8	117.3	114.7	115.6
C8-C9-C10	121.4	120.4	120.3
C10-C11-N1	119.5	119.0	118.9
C11-N1-O4	117.9	117.7	117.6
Dihedral Angle(deg)			
C1-O1-C2-O2	−5.7	2.10	3.20
O1-C2-C3-C4	125.1	42.7	42.5
O2-C2-C3-C4	−53.7	−137.0	−138.1
O2-C2-C3-C7	131.8	35.6	36.3
O1-C2-C3-C7	−49.3	−144.5	−142.9
C2-C3-C4-C5	4.0	−8.8	−3.6
C2-C3-C4-N1	−173.4	170.0	174.3
C3-C4-N1-C6	2.5	−4.6	1.0
C4-N1-C6-O3	179.3	−171,6	178.6
C5-C4-N1-C6	−175.2	174.3	179.1
C4-N1-C6-N2	−1.1	9.7	−1.3
N2-C7-C8-C9	−27.9	43.6	55.2
C8-C9-C10-C11	−0.5	1.2	0.7
C10-C11-N3-O4	−178.4	−179.5	179.8

The computational analysis revealed a prominence of planar structures; dihedral angles and geometric properties were similar. The calculated geometric parameters were also compared to the literature data. In published studies, C-O, C-N, and N-O bond lengths were recorded in the range of 1.215–1.219, 1.451–1.453, and 1.217–1.226 [71]. The calculated geometric parameters were in good agreement with the published data based on these experimental results.

Moreover, the IR spectra of the studied compounds were calculated (Figure 8); the frequency values of the studied compounds are given in Table 6. The frequency values of aromatic-aliphatic CH, NH, C=O and C=N groups corresponded to the vibrations at 3236–3241, 3580–3631, 1769–1782, and 1632–1678 cm^{-1}, respectively. The provided frequency values were in agreement with the literature data [71–74]. In addition, theoretical ^{1}H and ^{13}C NMR spectra were determined using the optimized structures; chemical shift values (Table 7) were calculated at the B3LYP-D3/6-311++G(d,p) level with reference to

tetramethylsilane (TMS). Both IR and NMR spectra proved that the structures in question were correct and in agreement with the experimental ones.

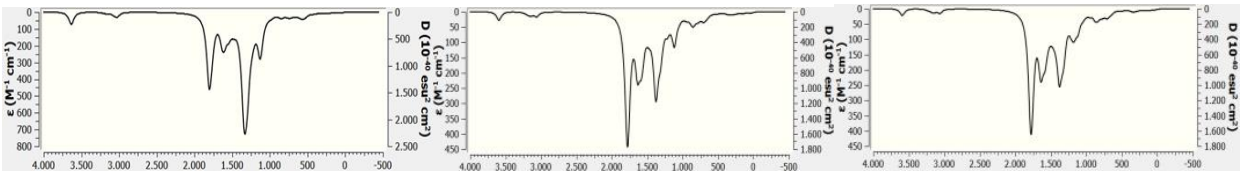

Figure 8. Calculated IR spectra of the studied compounds.

Table 6. Vibrational frequencies (cm^{-1}) of some functional groups in the studied compounds.

.	Assignment	1	2 (I)	2 (II)
▪	$\nu_{CHaromatic}$	3238	3243	3243
▪	$\nu_{CHaliphatic}$	3025	3147	3143
▪	ν_{NH}	3635	3595	3591
▪	$\nu_{C=O}$	1770	1788	1786
▪	ν_{C-O}	1130	1116	1113
▪	ν_{C-C}	1339	1315	1312
▪	$\nu_{C=C}$	1633	1635	1638
▪	$\nu_{C=N}$	-	1635	1638
▪	ν_{C-N}	1311	1378	1382
▪	ν_{N-O}	1550	1589	1594

Table 7. Spectral data for the studied compounds, calculated at the B3LYP-D3/6-311++G(d,p) level and experimental one.

Assignments	1	Experimental (1)	2 (I)	2 (II)	Experimental (2)
^{13}C-NMR					
C1	53.3	53.91	52.7	52.8	51.98
C2	164.7	152.16	162.6	163.2	165.60
C3	111.8	51.23	106.9	107.9	161.83
C4	134.9	149.94	155.5	173.2	148.12
C5	17.1	18.25	24.1	29.7	28.99
C6	142.9	165.92	148.1	147.2	162.12
C7	124.3	124.19	172.3	156.7	154.90

Table 7. *Cont.*

Assignments	1	Experimental (1)	2 (I)	2 (II)	Experimental (2)
C8	131.9	152.13	144.4	139.6	154.69
C9	115.8	98.39	127.8	123.4	123.42
C10	122.9	124.19	121.8	122.8	123.42
C11	142.0	157.11	147.0	147.5	144.82
C12	121.6	127.93	120.0	121.7	128.87
C13	121.1	127.93	124.9	126.2	128.87
^{1}H-NMR					
C1*H*′	3.91	3.54	3.93	3.84	3.49
C1*H*″	3.60	3.54	3.83	3.81	3.49
C1*H*‴	3.29	3.54	3.68	3.70	3.49
C5*H*′	2.82	2.27	2.99	3.03	2.46
C5*H*″	1.83	2.27	2.47	2.36	2.46
C5*H*‴	1.57	2.27	1.40	2.16	2.46
C9*H*	6.94	5.28–5.29	8.21	7.62	7.68–7.71
C10*H*	8.32	8.2–8.22	8.65	8.73	8.30–8.33
C12*H*	8.19	8.2–8.22	8.39	8.54	8.30–8.33
C13*H*	6.87	7.5–7.53	7.32	7.41	7.68–7.71
N1*H*	5.77	7.88	7.24	-	12.62
N2*H*	6.31	9.35	-	7.18	12.62

3.5.2. Electronic Properties

The study of the electronic features of molecules reveals vital information about their chemical properties. The molecular electrostatic potential (MEP) map, the MEP contour, and the contour plot of molecular orbitals are examples of techniques that can be used to understand these properties. Some of them are calculated and listed below.

Contour Plot of HOMO and LUMO

At the same theory level, the contour plot of the highest occupied molecular orbital (HOMO) and lowest unoccupied molecular orbital (LUMO) was calculated and represented in Figure 9.

HOMO and LUMO, which are known as boundary molecular orbitals, show the tendency to give and receive electrons. In the LUMO models, π-electrons were found to be generally delocalized over the whole structure of the two compounds. The HOMO structures revealed that the π-electrons were delocalized on the whole structure only in compound **1**, while they were concentrated on the dihydropyrimidine nucleus in **2** (Figure 9).

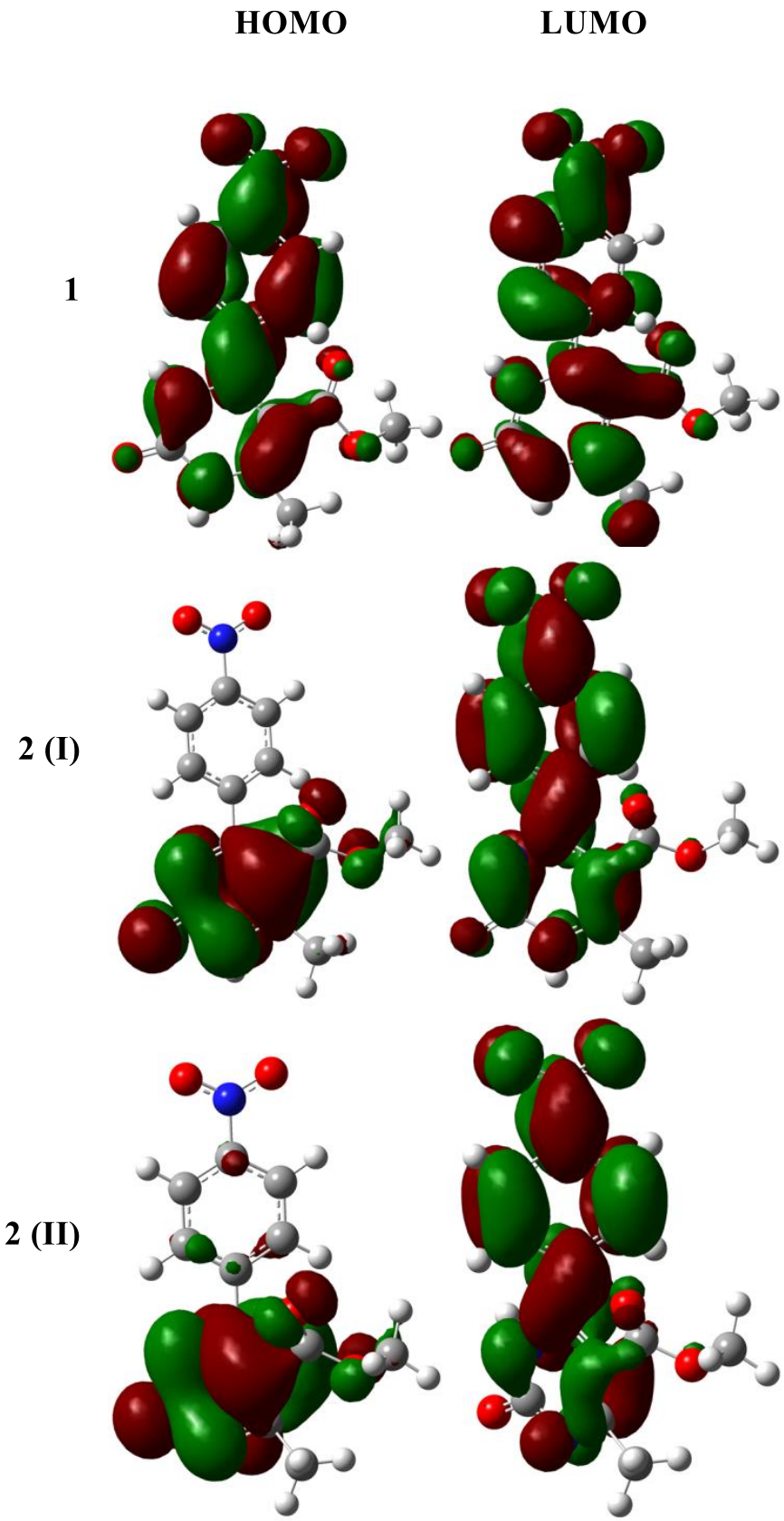

Figure 9. Contour diagram of frontier molecular orbitals.

MEP Maps

Molecular electrostatic potential (MEP) maps are a standard diagram used for describing the reactive sites of a compound. MEP maps can also be useful to locate nucleophilic and electrophilic active sites.

As shown in Figure 10, the yellow and red portions represent electron-rich regions, corresponding to the points where the oxygen atoms are located. Conversely, the regions with the poorest electron density are those around the dihydropyrimidine core.

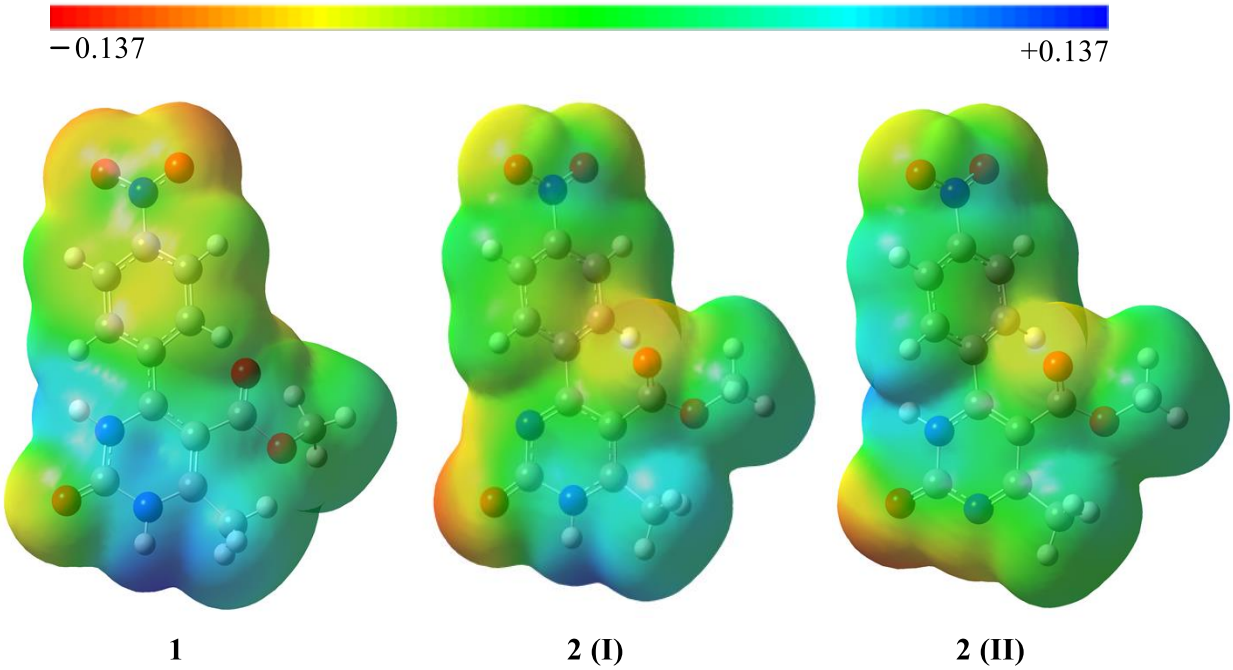

Figure 10. Molecular electrostatic potential maps calculated on the studied compounds.

3.5.3. Molecular Docking

The biological reactivity of chemicals can be predicted by using in silico techniques; the best choice in these analyses is molecular docking. The antimycotic effect of the synthesized compounds was experimentally studied against clinically relevant fungal strains, and **2** was found to be superior to its precursor. To identify a putative target for these compounds, an extensive literature survey was carried out to identify novel drug targets deemed essential for parasite growth and survival. Among them, we selected the putative target chitin deacetylase (AngCDA) from *Aspergillus niger*, considering that some pyrimidine derivatives were found to be able to inhibit this enzyme [75]. Hence, the biological activity of the compounds was investigated by molecular docking calculations, using the model deposited under accession code 7BLY in the Protein Data Bank (PDB) [60]. The studied compounds and the target protein were re-minimized using the OPLS4 method. The x-y-z coordinates of the receptor-binding domain were defined as 15.3, 41.74, and -30.61, respectively. The calculations showed that the compounds may inhibit the selected target. Docking structures and the interaction map of each compound are represented in Figure 11. Additionally, docking score (DS), van der Walls energy (E_{vdW}), coulomb energy (E_{Coul}), and total interaction energy (E_{Total}) are given in Table 8.

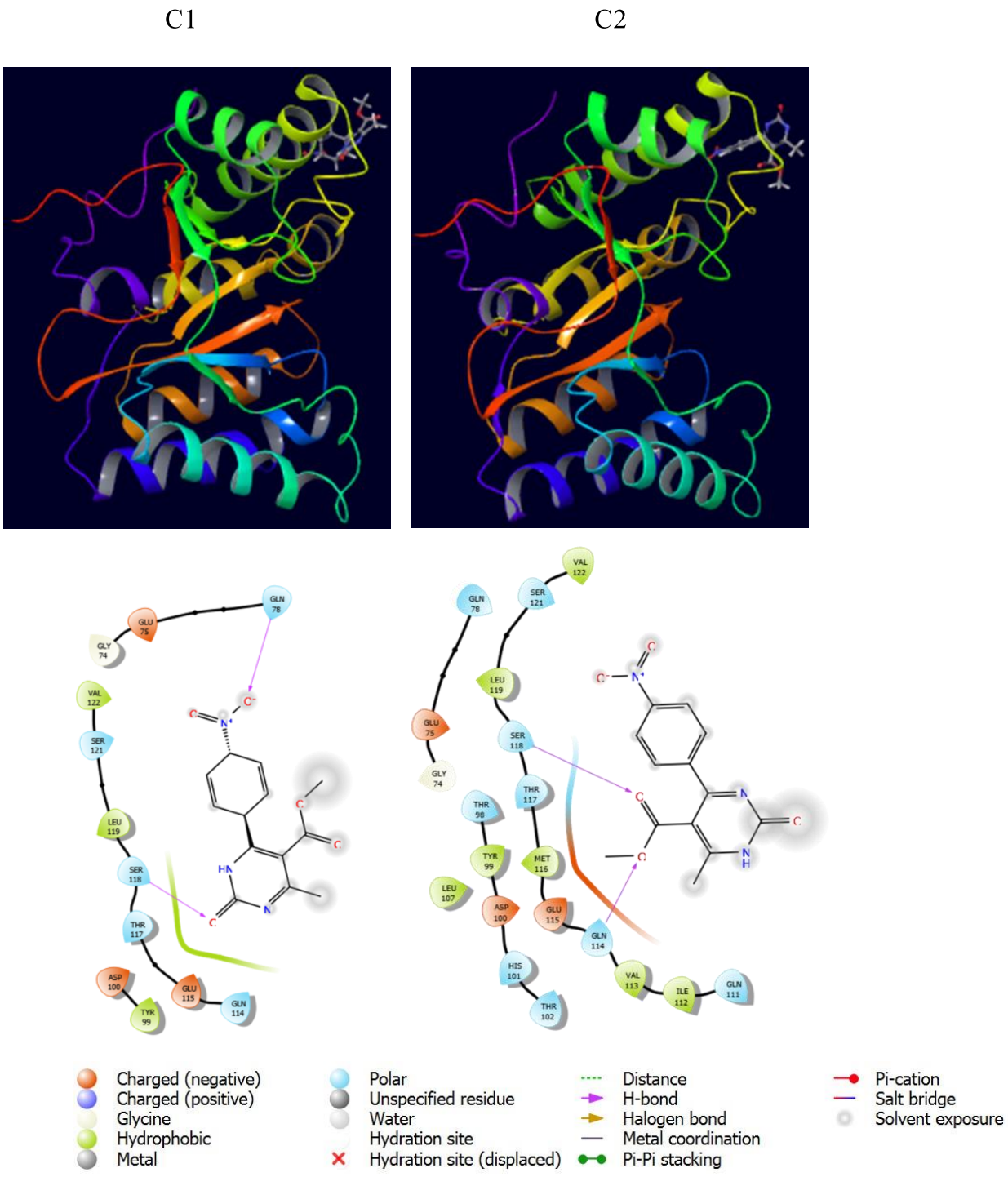

Figure 11. The docking structures and interaction maps of studied compounds.

Table 8. Molecular docking results.

Compound	DS [a]	E_{vdW} [a]	E_{Coul} [a]	E_{Total} [a]
1	−3.022	−19.294	−6.132	−25.427
2	−3.351	−20.298	−6.055	−26.353
Fluconazole	−3.154	−19.563	−4.839	−24.402

[a] in kcal/mol

Data reported in Figure 11 and Table 8 evidenced that the studied compounds have a good binding affinity for the target protein. Furthermore, the fact that the whole parameters of **2** were better than those of **1**, except for the Coulomb interactions, could be in agreement with its higher biological activity (Table 8).

4. Conclusions

Methyl 6-methyl-4-(4-nitrophenyl)-2-oxo-1,2-dihydropyrimidine-5-carboxylate **2** was obtained by the regioselective oxidative dehydrogenation of dihydropyrimidine **1** in the presence of cerium ammonium nitrate (CAN). Its structure was investigated by various methods, including NMR spectroscopy and SC-XRD. These techniques allowed us to determine the tautomeric form of the title compound. Moreover, the presence of non-covalent interactions and their impact on the crystal packing were studied by Hirshfeld surface and contact enrichment analysis. Furthermore, the studied compounds were investigated by computational techniques at the B3LYP-D3/6-311++G(d,p) level: their structural, spectral, and electronic properties were investigated. Finally, considering that dihydropyrimidines are privileged scaffolds in medicinal chemistry, the biological activity of the synthesized compounds was investigated against *Candida albicans*, *Aspergillus flavus*, and *Aspergillus niger* revealing an efficacy comparable to or even higher than that of the established antimycotic fluconazole. Moreover, molecular docking calculations were performed against a putative target from *Aspergillus niger*.

Supplementary Materials: The following supporting information can be downloaded at: https://www.mdpi.com/article/10.3390/cryst13010052/s1. Figure S1. 1H NMR spectrum of the synthesized dihydropyrimidine 1. Figure S2. ^{13}C NMR spectrum of the synthesized dihydropyrimidine **1**. Figure S3. 1H NMR spectrum of the synthesized dihydropyrimidine 2. Figure S4. 13C NMR spectrum of the synthesized dihydropyrimidine 2. Table S1. Bond lengths [Å] and angles [°] for the crystal structure of 2. Figure S5. 2D HS Fingerprint plots of 2, providing a visual summary of the frequency of each combination of de and di across the HS. Points with a contribution to the surface are colored blue for a small contribution to green for a great contribution.

Author Contributions: Synthesis, A.H.; NMR and mass investigations, A.H.; Formal analysis, A.H.; Single crystal structure description, M.M. and F.M.; Hirshfeld surface analysis, M.M. and F.M.; Antifungal studies, A.I. and L.R.C.; Computational approach, E.G. and K.S.; Mass analysis, M.D.; Supervision, U.H.; Funding acquisition, U.H.; Project administration, U.H.; Writing—Original Draft, A.H., M.M., F.M., A.I., E.G., K.S., M.D., U.H. and V.A.; Writing—Review & Editing, A.H., M.M., F.M., A.I., L.R.C. and M.D. All authors have read and agreed to the published version of the manuscript.

Funding: This work was supported by the Erasmus + overseas/ICM KA107 program, Science Development Foundation under the President of the Republic of Azerbaijan and TUBITAK in the frames of the project number EİF-BGM-5-AZTURK-1/2018-2/02/4-M-02 and by the Scientific Research Project Fund of Sivas Cumhuriyet University under the project number RGD-020.

Data Availability Statement: Data sharing not applicable.

Conflicts of Interest: The authors declare that they have no known competing financial interests or personal relationships that could have appeared to influence the work reported in this paper.

References

1. Tron, G.C.; Minassi, A.; Appendino, G. Pietro Biginelli: The Man Behind the Reaction. *Eur. J. Org. Chem.* **2011**, *2011*, 5541–5550. [CrossRef]
2. Huseynzada, A.E.; Jelsch, C.; Akhundzada, H.N.; Soudani, S.; Ben Nasr, C.; Doria, F.; Hasanova, U.A.; Freccero, M. Synthesis, crystal structure and antibacterial properties of 6-methyl-2-oxo-4-(quinolin-2-yl)-1,2,3,4-tetrahydropyrimidine-5-carboxylate. *J. Mol. Struct.* **2020**, *1219*, 128581. [CrossRef]
3. Stucchi, M.; Lesma, G.; Meneghetti, F.; Rainoldi, G.; Sacchetti, A.; Silvani, A. Organocatalytic Asymmetric Biginelli-like Reaction Involving Isatin. *J. Org. Chem.* **2016**, *81*, 1877–1884. [CrossRef] [PubMed]
4. Huseynzada, A.E.; Jelsch, C.; Akhundzada, H.N.; Soudani, S.; Nasr, C.B.; Doria, F.; Hasanova, U.A.; Freccero, M.; Gakhramanova, Z.; Ganbarov, K.; et al. Synthesis, crystal structure and antibacterial studies of 2,4,6-trimetoxybenzaldehyde based dihydropyrimidine derivatives. *J. Mol. Struct.* **2021**, *1241*, 130678. [CrossRef]

5. Kappe, C.O. Recent advances in the Biginelli dihydropyrimidine synthesis. New tricks from an old dog. *Acc. Chem. Res.* **2000**, *33*, 879–888. [CrossRef]
6. Li, S.; Zhao, G.; Xia, G.; Wang, L.; Zheng, Z.; Xie, Y.; Zhong, W.; Xiao, J.; Li, X.; Cui, H. Dihydropyrimidine Compounds and Their Uses in Preparation of Medicaments for Treating and Preventing Antiviral Diseases. U.S. Patent No. 8,168,642, 1 May 2012.
7. Watabe, T.; Ogura, K.; Nishiyama, T. Molecular Toxicological Mechanism of the Lethal Interactions of the New Antiviral Drug, Sorivudine, with 5-Fluorouracil Prodrugs and Genetic Deficiency of Dihydropyrimidine Dehydrogenase. *Yakugaku Zasshi* **2002**, *122*, 527–535. [CrossRef]
8. Awadallah, F.M.; Piazza, G.A.; Gary, B.D.; Keeton, A.B.; Canzoneri, J.C. Synthesis of some dihydropyrimidine-based compounds bearing pyrazoline moiety and evaluation of their antiproliferative activity. *Eur. J. Med. Chem.* **2013**, *70*, 273–279. [CrossRef]
9. Oie, S.; Ono, M.; Fukushima, H.; Hosoi, F.; Yano, H.; Maruyama, Y.; Kojiro, M.; Terada, T.; Hirano, K.; Kuwano, M.; et al. Alteration of dihydropyrimidine dehydrogenase expression by IFN-α affects the antiproliferative effects of 5-fluorouracil in human hepatocellular carcinoma cells. *Mol. Cancer Ther.* **2007**, *6*, 2310–2318. [CrossRef]
10. Klein, E.; DeBonis, S.; Thiede, B.; Skoufias, D.A.; Kozielski, F.; Lebeau, L. New chemical tools for investigating human mitotic kinesin Eg5. *Bioorg. Med. Chem.* **2007**, *15*, 6474–6488. [CrossRef]
11. Kaan, H.Y.K.; Ulaganathan, V.; Rath, O.; Prokopcovà, H.; Dallinger, D.; Kappe, C.O.; Kozielski, F. Structural basis for inhibition of Eg5 by dihydropyrimidines: Stereoselectivity of antimitotic inhibitors enastron, dimethylenastron and fluorastrol. *J. Med. Chem.* **2010**, *53*, 5676–5683. [CrossRef]
12. Wright, C.M.; Chovatiya, R.J.; Jameson, N.E.; Turner, D.M.; Zhu, G.; Werner, S.; Huryn, D.M.; Pipas, J.M.; Day, B.W.; Wipf, P.; et al. Pyrimidinone-peptoid hybrid molecules with distinct effects on molecular chaperone function and cell proliferation. *Bioorg. Med. Chem.* **2008**, *16*, 3291–3301. [CrossRef] [PubMed]
13. Agbaje, O.C.; Fadeyi, O.O.; Fadeyi, S.A.; Myles, L.E.; Okoro, C.O. Synthesis and in vitro cytotoxicity evaluation of some fluorinated hexahydropyrimidine derivatives. *Bioorg. Med. Chem. Lett.* **2011**, *21*, 989–992. [CrossRef]
14. Kumar, B.R.P.; Sankar, G.; Baig, R.B.N.; Chandrashekaran, S. Novel Biginelli dihydropyrimidines with potential anticancer activity: A parallel synthesis and CoMSIA study. *Eur. J. Med. Chem.* **2009**, *44*, 4192–4198. [CrossRef]
15. Ibrahim, D.A.; El-Metwally, A.M. Design, synthesis, and biological evaluation of novel pyrimidine derivatives as CDK2 inhibitors. *Eur. J. Med. Chem.* **2010**, *45*, 1158–1166. [CrossRef] [PubMed]
16. Wang, A.; Liu, X.; Su, Z.; Jing, H. New magnetic nanocomposites of ZrO_2–Al_2O_3–Fe_3O_4 as green solid acid catalysts in organic reactions. *Catal. Sci. Technol.* **2013**, *4*, 71–80. [CrossRef]
17. Ghosh, B.K.; Hazra, S.; Ghosh, N.N. Synthesis of Cu@CF@SBA15: A Versatile catalysts for (i) reduction of dyes, trifluralin, Synthesis of (ii) DHPMs by Biginelli reaction and (iii) 1,2,3-triazole derivatives by 'Click reaction'. *Catal. Commun.* **2016**, *80*, 44–48. [CrossRef]
18. October, N.; Watermeyer, N.D.; Yardley, V.; Egan, T.J.; Ncokazi, K.; Chibale, K. Reversed Chloroquines Based on the 3,4-Dihydropyrimidin-2(1H)-one Scaffold: Synthesis and Evaluation for Antimalarial, β-Haematin Inhibition, and Cytotoxic Activity. *ChemMedChem* **2008**, *3*, 1649–1653. [CrossRef]
19. Fatima, S.; Sharma, A.; Saxena, R.; Tripathi, R.; Shukla, S.K.; Pandey, S.K.; Tripathi, R.; Tripathi, R.P. One pot efficient diversity oriented synthesis of polyfunctional styryl thiazolopyrimidines and their bio-evaluation as antimalarial and anti-HIV agents. *Eur. J. Med. Chem.* **2012**, *55*, 195–204. [CrossRef] [PubMed]
20. Kaur, H.; Machado, M.; De Kock, C.; Smith, P.; Chibale, K.; Prudêncio, M.; Singh, K. Primaquine–pyrimidine hybrids: Synthesis and dual-stage antiplasmodial activity. *Eur. J. Med. Chem.* **2015**, *101*, 266–273. [CrossRef]
21. Akhaja, T.N.; Raval, J.P. 1,3-dihydro-2H-indol-2-ones derivatives: Design, Synthesis, in vitro antibacterial, antifungal and antitubercular study. *Eur. J. Med. Chem.* **2011**, *46*, 5573–5579. [CrossRef]
22. Yadlapalli, R.K.; Chourasia, O.P.; Vemuri, K.; Sritharan, M.; Perali, R.S. Synthesis and in vitro anticancer and antitubercular activity of diarylpyrazole ligated dihydropyrimidines possessing lipophilic carbamoyl group. *Bioorg. Med. Chem. Lett.* **2012**, *22*, 2708–2711. [CrossRef] [PubMed]
23. Mokale, S.N.; Shinde, S.S.; Elgire, R.D.; Sangshetti, J.N.; Shinde, D.B. Synthesis and anti-inflammatory activity of some 3-(4,6-disubtituted-2-thioxo-1,2,3,4-tetrahydropyrimidin-5-yl) propanoic acid derivatives. *Bioorg. Med. Chem. Lett.* **2010**, *20*, 4424–4426. [CrossRef] [PubMed]
24. Bahekar, S.S.; Shinde, D.B. Synthesis and anti-inflammatory activity of some [2-amino-6-(4-substituted aryl)-4-(4-substituted phenyl)-1,6-dihydropyrimidine-5-yl]-acetic acid derivatives. *Acta Pharm.* **2003**, *53*, 223–229. [PubMed]
25. Bahekar, S.S.; Shinde, D.B. Synthesis and anti-inflammatory activity of some [4,6-(4-substituted aryl)-2-thioxo-1,2,3,4-tetrahydro-pyrimidin-5-yl]-acetic acid derivatives. *Bioorg. Med. Chem. Lett.* **2004**, *14*, 1733–1736. [CrossRef]
26. Terracciano, S.; Lauro, G.; Strocchia, M.; Fischer, K.; Werz, O.; Riccio, R.; Bruno, I.; Bifulco, G. Structural insights for the optimization of dihydropyrimidin-2(1 H)-one based mPGES-1 inhibitors. *ACS Med. Chem. Lett.* **2015**, *6*, 187–191. [CrossRef]
27. Trivedi, A.R.; Bhuva, V.R.; Dholariya, B.H.; Dodiya, D.K.; Kataria, V.B.; Shah, V.H. Novel dihydropyrimidines as a potential new class of antitubercular agents. *Bioorg. Med. Chem. Lett.* **2010**, *20*, 6100–6102. [CrossRef]
28. Cazzaniga, G.; Mori, M.; Chiarelli, L.R.; Gelain, A.; Meneghetti, F.; Villa, S. Natural products against key Mycobacterium tuberculosis enzymatic targets: Emerging opportunities for drug discovery. *Eur. J. Med. Chem.* **2021**, *224*, 113732. [CrossRef]

29. Maharramov, A.M.; Ramazanov, M.A.; Guliyeva, G.A.; Huseynzada, A.E.; Hasanova, U.A.; Shikhaliyev, N.G.; Eyvazova, G.M.; Hajiyeva, S.F.; Mamedov, I.G.; Aghayev, M.M. Synthesis, investigation of the new derivatives of dihydropyrimidines and determination of their biological activity. *J. Mol. Struct.* **2017**, *1141*, 39–43. [CrossRef]
30. Rashid, U.; Sultana, R.; Shaheen, N.; Hassan, S.F.; Yaqoob, F.; Ahmad, M.J.; Iftikhar, F.; Sultana, N.; Asghar, S.; Yasinzai, M.; et al. Structure based medicinal chemistry-driven strategy to design substituted dihydropyrimidines as potential antileishmanial agents. *Eur. J. Med. Chem.* **2016**, *115*, 230–244. [CrossRef]
31. Atwal, K.S.; Rovnyak, G.C.; Schwartz, J.; Moreland, S.; Hedberg, A.; Gougoutas, J.Z.; Malley, M.F.; Floyd, D.M. Dihydropyrimidine Calcium Channel Blockers: 2-Heterosubstituted 4-Aryl-l,4-dihydro-6-methyl-5-pyrimidinecarboxylic Acid Esters as Potent Mimics of Dihydropyridines. *J. Med. Chem.* **1990**, *33*, 1510–1515. [CrossRef]
32. Zorkun, I.S.; Saraç, S.; Çelebi, S.; Erol, K. Synthesis of 4-aryl-3,4-dihydropyrimidin-2(1H)-thione derivatives as potential calcium channel blockers. *Bioorg. Med. Chem.* **2006**, *14*, 8582–8589. [CrossRef] [PubMed]
33. Chikhale, R.V.; Bhole, R.P.; Khedekar, P.B.; Bhusari, K.P. Synthesis and pharmacological investigation of 3-(substituted 1-phenylethanone)-4-(substituted phenyl)-1, 2, 3, 4-tetrahydropyrimidine-5-carboxylates. *Eur. J. Med. Chem.* **2009**, *44*, 3645–3653. [CrossRef]
34. Lewis, R.W.; Mabry, J.; Polisar, J.G.; Eagen, K.P.; Ganem, B.; Hess, G.P. Dihydropyrimidinone positive modulation of δ-subunit-containing γ-aminobutyric acid type a receptors, including an epilepsy-linked mutant variant. *Biochemistry* **2010**, *49*, 4841–4851. [CrossRef] [PubMed]
35. Figueroa-Valverde, L.; Díaz-Cedillo, F.; López-Ramos, M.; Garcia-Cervera, E. Activity induced by two steroid-dihydropyrimidine derivatives on glucose levels in a diabetic rat model. relationship between descriptors logP and π and its Antidiabetic activity. *Int. J. PharmTech Res.* **2010**, *2*, 2075–2080.
36. Patel, A.D.; Barot, R.; Parmar, I.; Panchal, I.; Shah, U.; Patel, M.; Mishtry, B. Molecular Docking, In-Silico ADMET Study and Development of 1,6- Dihydropyrimidine Derivative as Protein Tyrosine Phosphatase Inhibitor: An Approach to Design and Develop Antidiabetic Agents. *Curr. Comput. Aided Drug Des.* **2018**, *14*, 349–362. [CrossRef]
37. Bairagi, K.M.; Younis, N.S.; Emeka, P.M.; Sangtani, E.; Gonnade, R.G.; Venugopala, K.N.; Alwassil, O.I.; Khalil, H.E.; Nayak, S.K. Antidiabetic Activity of Dihydropyrimidine Scaffolds and Structural Insight by Single Crystal X-ray Studies. *Med. Chem.* **2019**, *16*, 996–1003. [CrossRef]
38. Bairagi, K.M.; Younis, N.S.; Emeka, P.M.; Venugopala, K.N.; Alwassil, O.I.; Khalil, H.E.; Sangtani, E.; Gonnade, R.G.; Mohanlall, V.; Nayak, S.K. Chemistry, anti-diabetic activity and structural analysis of substituted dihydropyrimidine analogues. *J. Mol. Struct.* **2021**, *1227*, 129412. [CrossRef]
39. Patil, A.D.; Kumar, N.V.; Kokke, W.C.; Bean, M.F.; Freyer, A.J.; De Brosse, C.; Mai, S.; Truneh, A.; Faulkner, D.J.; Carte, B.; et al. Novel Alkaloids from the Sponge Batzella sp.: Inhibitors of HIV gp120-Human CD4 Binding. *J. Org. Chem.* **1995**, *60*, 1182–1188. [CrossRef]
40. Mehta, K.B.; Patel, R.K.; Joshi, H.S. In silico study of novel Dihydropyrimidines against Anti Cancer, Anti Tuberculosis, Anti HIV and Anti Malarial activity. *Int. J. Sci. Eng. Res.* **2013**, *4*, 1–8.
41. Bairagi, K.M.; Venugopala, K.N.; Mondal, P.K.; Gleiser, R.M.; Chopra, D.; García, D.; Odhav, B.; Nayak, S.K. Larvicidal study of tetrahydropyrimidine scaffolds against Anopheles arabiensis and structural insight by single crystal X-ray studies. *Chem. Biol. Drug Des.* **2018**, *92*, 1924–1932. [CrossRef]
42. Singh, B.K.; Mishra, M.; Saxena, N.; Yadav, G.P.; Maulik, P.R.; Sahoo, M.K.; Gaur, R.L.; Murthy, P.K.; Tripathi, R.P. Synthesis of 2-sulfanyl-6-methyl-1,4-dihydropyrimidines as a new class of antifilarial agents. *Eur. J. Med. Chem.* **2008**, *43*, 2717–2723. [CrossRef] [PubMed]
43. Barrow, J.C.; Nantermet, P.G.; Selnick, H.G.; Glass, K.L.; Rittle, K.E.; Gilbert, K.F.; Steele, T.G.; Homnick, C.F.; Freidinger, R.M.; Ransom, R.W.; et al. In vitro, and in vivo, evaluation of dihydropyrimidinone C-5 amides as potent and selective α(1A) receptor antagonists for the treatment of benign prostatic hyperplasia. *J. Med. Chem.* **2000**, *43*, 2703–2718. [CrossRef] [PubMed]
44. Zhu, X.; Zhao, G.; Zhou, X.; Xu, X.; Xia, G.; Zheng, Z.; Wang, L.; Yang, X.; Li, S. 2,4-Diaryl-4,6,7,8-tetrahydroquinazolin-5(1H)-one derivatives as anti-HBV agents targeting at capsid assembly. *Bioorg. Med. Chem. Lett.* **2010**, *20*, 299–301. [CrossRef] [PubMed]
45. Rovnyak, G.C.; Atwal, K.S.; Kimball, S.D.; O'Reilly, B.C.; Schwartz, J.; Hedberg, A.; Moreland, S.; Gougoutas, J.Z.; Malley, M.F. Dihydropyrimidine Calcium Channel Blockers. 4. Basic 3-Substituted-4-aryl-1,4-dihydropyrimidine-5-Carboxylic Acid Esters. Potent Antihypertensive Agents. *J. Med. Chem.* **1992**, *35*, 3254–3263. [CrossRef] [PubMed]
46. Finlay, H.J.; Lloyd, J.; Vaccaro, W.; Kover, A.; Yan, L.; Bhave, G.; Prol, J.; Huynh, T.; Bhandaru, R.; Caringal, Y.; et al. Discovery of ((S)-5-(methoxymethyl)-7-(1-methyl-1 H -indol-2-yl)-2- (trifluoromethyl)-4,7-dihydropyrazolo[1 ,5- a]pyrimidin-6-yl)((S)-2-(3-methylisoxazol-5-yl)pyrrolidin-1-yl)methanone as a potent and selective I Kur inhibitor. *J. Med. Chem.* **2012**, *55*, 3036–3048. [CrossRef] [PubMed]
47. Lloyd, J.; Finlay, H.J.; Vacarro, W.; Hyunh, T.; Kover, A.; Bhandaru, R.; Yan, L.; Atwal, K.; Conder, M.L.; Jenkins-West, T.; et al. Pyrrolidine amides of pyrazolodihydropyrimidines as potent and selective KV1.5 blockers. *Bioorg. Med. Chem. Lett.* **2010**, *20*, 1436–1439. [CrossRef] [PubMed]
48. Lloyd, J.; Finlay, H.J.; Atwal, K.; Kover, A.; Prol, J.; Yan, L.; Bhandaru, R.; Vaccaro, W.; Huynh, T.; Huang, C.S.; et al. Dihydropyrazolopyrimidines containing benzimidazoles as KV1.5 potassium channel antagonists. *Bioorg. Med. Chem. Lett.* **2009**, *19*, 5469–5473. [CrossRef]

49. Wong, W.C.; Sun, W.; Lagu, B.; Tian, D.; Marzabadi, M.R.; Zhang, F.; Nagarathnam, D.; Miao, S.W.; Wetzel, J.M.; Peng, J.; et al. Design and synthesis of novel α(1a) adrenoceptor-selective antagonists. 4. Structure-activity relationship in the dihydropyrimidine series. *J. Med. Chem.* **1999**, *42*, 4804–4813. [CrossRef] [PubMed]
50. Huseynzada, A.E.; Jelch, C.; Akhundzada, H.V.N.; Soudani, S.; Ben Nasr, C.; Israyilova, A.; Doria, F.; Hasanova, U.A.; Khankishiyeva, R.F.; Freccero, M. Synthesis, crystal structure and antibacterial studies of dihydropyrimidines and their regioselectively oxidized products. *RSC Adv.* **2021**, *11*, 6312–6329. [CrossRef]
51. Duarte, H.A.; Carvalho, S.; Paniago, E.B.; Simas, A.M. Importance of Tautomers in the Chemical Behavior of Tetracyclines. *J. Pharm. Sci.* **1999**, *88*, 111–120. [CrossRef]
52. Sheldrick, G.M. *SHELXTL V5.1, Software Reference Manual*; Bruker AXS Inc.: Madison, WI, USA, 1997; pp. 1–250.
53. Farrugia, L.J. IUCr WinGX and ORTEP for Windows: An update. *J. Appl. Crystallogr.* **2012**, *45*, 849–854. [CrossRef]
54. MacRae, C.F.; Sovago, I.; Cottrell, S.J.; Galek, P.T.A.; McCabe, P.; Pidcock, E.; Platings, M.; Shields, G.P.; Stevens, J.S.; Towler, M.; et al. Mercury 4.0: From visualization to analysis, design and prediction. *J. Appl. Crystallogr.* **2020**, *53*, 226–235. [CrossRef] [PubMed]
55. Nardelli, M. Parst: A system of fortran routines for calculating molecular structure parameters from results of crystal structure analyses. *Comput. Chem.* **1983**, *7*, 95–98. [CrossRef]
56. Spackman, P.R.; Turner, M.J.; McKinnon, J.J.; Wolff, S.K.; Grimwood, D.J.; Jayatilaka, D.; Spackman, M.A. CrystalExplorer: A program for Hirshfeld surface analysis, visualization and quantitative analysis of molecular crystals. *J. Appl. Crystallogr.* **2021**, *54*, 1006–1011. [CrossRef]
57. Jelsch, C.; Ejsmont, K.; Huder, L. The enrichment ratio of atomic contacts in crystals, an indicator derived from the Hirshfeld surface analysis. *IUCrJ* **2014**, *1*, 119–128. [CrossRef] [PubMed]
58. Rex, J.H.; Ghannoum, M.A.; Alexander, B.D.; Knapp, C.C.; Andes, D.; Motyl, M.R.; Arthington-Skaggs, B.; Ostroski-Zeichner, L.; Brown, S.D.; Pfaller, M. *M38-A2 Reference Method for Broth Dilution Antifungal Susceptibility Testing of Filamentous Fungi; Approved Standard-Second Edition*, 2nd ed.; Clinical and Laboratory Standards Institute: Wayne, PA, USA, 2008; ISBN 610.688.0700.
59. Borman, A.M.; Fraser, M.; Palmer, M.D.; Szekely, A.; Houldsworth, M.; Patterson, Z.; Johnson, E.M. MIC Distributions and Evaluation of Fungicidal Activity for Amphotericin B, Itraconazole, Voriconazole, Posaconazole and Caspofungin and 20 Species of Pathogenic Filamentous Fungi Determined Using the CLSI Broth Microdilution Method. *J. Fungi* **2017**, *3*, 27. [CrossRef] [PubMed]
60. Bonin, M.; Hameleers, L.; Hembach, L.; Roret, T.; Cord-Landwehr, S.; Michel, G.; Moerschbacher, B.M. In silico and in vitro analysis of an Aspergillus niger chitin deacetylase to decipher its subsite sugar preferences. *J. Biol. Chem.* **2021**, *297*, 101129. [CrossRef] [PubMed]
61. Mouyna, I.; Dellière, S.; Beauvais, A.; Gravelat, F.; Snarr, B.; Lehoux, M.; Zacharias, C.; Sun, Y.; Carrion, S.D.J.; Pearlman, E.; et al. What Are the Functions of Chitin Deacetylases in Aspergillus fumigatus? *Front. Cell Infect. Microbiol.* **2020**, *10*, 28. [CrossRef]
62. Bairagi, K.M.; Ingle, K.S.; Bhowal, R.; Mohurle, S.A.; Hasija, A.; Alwassil, O.I.; Venugopala, K.N.; Chopra, D.; Nayak, S.K. Interplay of Halogen and Hydrogen Bonding through Co–Crystallization in Pharmacologically Active Dihydropyrimidines: Insights from Crystal Structure and Energy Framework. *Chempluschem* **2021**, *86*, 1167–1176. [CrossRef]
63. Ciceri, S.; Colombo, D.; Ferraboschi, P.; Grisenti, P.; Iannone, M.; Mori, M.; Meneghetti, F. Vecuronium bromide and its advanced intermediates: A crystallographic and spectroscopic study. *Steroids* **2021**, *176*, 108928. [CrossRef]
64. Mori, M.; Fumagalli, E.; Castellano, C.; Tresoldi, A.; Sacchetti, A.; Meneghetti, F. Synthesis and characterization of a tetradentate bispidine-based ligand and its zinc(II) complex. *Inorg. Chim. Acta* **2022**, *538*, 120968. [CrossRef]
65. Dugoni, G.C.; Mori, M.; Dichiarante, V.; Sacchetti, A.; Meneghetti, F. Synthesis and characterization of a novel lanthanum (III) complex with a di(2-picolyl)amine-based ligand endowed with fluorescent properties. *J. Mol. Struct.* **2022**, *1265*, 133398. [CrossRef]
66. Monteiro, M.C.; De La Cruz, M.; Cantizani, J.; Moreno, C.; Tormo, J.R.; Mellado, E.; De Lucas, J.R.; Asensio, F.; Valiante, V.; Brakhage, A.A.; et al. A New Approach to Drug Discovery: High-Throughput Screening of Microbial Natural Extracts against Aspergillus fumigatus Using Resazurin. *SLAS Discov.* **2012**, *17*, 542–549. [CrossRef] [PubMed]
67. Nenaah, G. Antibacterial and antifungal activities of (beta)-carboline alkaloids of Peganum harmala (L) seeds and their combination effects. *Fitoterapia* **2010**, *81*, 779–782. [CrossRef]
68. Cruz, K.S.; Lima, E.S.; da Silva, M.D.J.A.; de Souza, E.S.; Montoia, A.; Pohlit, A.M.; Souza, J.V.B. De Screening and antifungal activity of a β-carboline derivative against cryptococcus neoformans and C. gattii. *Int. J. Microbiol.* **2019**, *2019*, 7157845. [CrossRef]
69. Li, Z.; Chen, S.; Zhu, S.; Luo, J.; Zhang, Y.; Weng, Q. Synthesis and Fungicidal Activity of β-Carboline Alkaloids and Their Derivatives. *Molecules* **2015**, *20*, 13941–13957. [CrossRef]
70. Huseynzada, A.; Mori, M.; Meneghetti, F.; Israyilova, A.; Tuzun, G.; Sayin, K.; Chiarelli, L.R.; Mutlu, C.; Demiralp, M.; Hasanova, U.; et al. Synthesis, crystal structure, Hirshfeld surface, computational and antibacterial studies of a 9-phenanthrenecarboxaldehyde-based thiodihydropyrimidine derivative. *J. Mol. Struct.* **2022**, *1267*, 133571. [CrossRef]
71. Dikmen, G.; Hür, D. Synthesis, spectroscopic characterization and theoretical studies of (4-boronobenzoyl)serine. *Chem. Phys.* **2020**, *530*, 110601. [CrossRef]
72. Tüzün, B.; Sayin, K. Investigations over optical properties of boron complexes of benzothiazolines. *Spectrochim. Acta Part A Mol. Biomol. Spectrosc.* **2019**, *208*, 48–56. [CrossRef]

73. Sayin, K.; Üngördü, A. Investigations of structural, spectral and electronic properties of enrofloxacin and boron complexes via quantum chemical calculation and molecular docking. *Spectrochim. Acta Part A Mol. Biomol. Spectrosc.* **2019**, *220*, 117102. [CrossRef]
74. Wang, L.; Cao, C.; Cao, C. Substituent effects on the stretching vibration of C=N in multi-substituted benzylideneanilines. *J. Phys. Org. Chem.* **2019**, *32*, e3969. [CrossRef]
75. Garcia, A.P.; Cruz, J.M.; Zanni, R.; Hinojosa, D.F.R.; Ortuno, D.F.; Llompart, M.G.; Domenech, R.G.; Alvarez, J.G. *Chitin Deacetylase Inhibitors and Use Thereof as Agricultural Fungicides, Arthropocides and Nematicides*; WIPO: Geneva, Switzerland, 2020; pp. 1–72.